Open access • Journal Article • DOI:10.1007/BF02156765

Infra-red Tomography of Port-wine-stain Blood Vessels in Human Skin

J.S. Nelson, Thomas E. Milner, B. S. Tanenbaum, Dennis M. Goodman ...+1 more authors

Institutions: University of California, Irvine, Harvey Mudd College, Lawrence Livermore National Laboratory, University of Amsterdam

Published on: 01 Sep 1996 - Lasers in Medical Science (Springer-Verlag)

Title
Infra-red tomography of port-wine-stain blood vessels in human skin

Journal
Lasers in Medical Science, 11(3)

ISSN
0268-8921

Authors
Nelson, JS
Milner, TE
Tanenbaum, BS
et al.

Publication Date
1996-09-01

DOI
10.1007/BF02156765

Lasers in Medical Science 1996, **11**:199–204

Infra-red Tomography of Port-wine-stain Blood Vessels in Human Skin

J.S. NELSON[a], T.E. MILNER[a], B.S. TANENBAUM[b], D.M. GOODMAN[c], M.J.C. VAN GEMERT[d]

[a]*Beckman Laser Institute and Medical Clinic, University of California, Irvine, CA 92612, USA*
[b]*Department of Engineering, Harvey Mudd College, Claremont, CA 91711, USA*
[c]*Imaging Sciences Division, Lawrence Livermore National Laboratory, Livermore, CA 94550, USA*
[d]*Laser Center, Academic Medical Center, University of Amsterdam, The Netherlands*

Correspondence to J. Stuart Nelson, Beckman Laser Institute and Medical Clinic, University of California, Irvine, 1002 Health Sciences Road East, Irvine, CA 92612, USA

Paper received 22 May 1996

Abstract. Specifying the distribution of laser energy within a tissue is the first step towards understanding and capitalizing on a variety of laser–tissue interactions. Whether photothermal, photochemical or photomechanical in nature, laser–tissue interactions begin with the absorption of photon energy. The spatial distribution of photon absorption specifies the required laser exposure to be delivered and the extent of subsequent therapeutic action. Using infra-red tomography (IRT), the broad, long-term objective of this research is the development of a tomographic reconstruction algorithm as a means to determine: (1) the depths and physical dimensions of discrete subsurface port-wine-stain (PWS) blood vessels in human skin; and (2) the initial space-dependent temperature increase in PWS blood vessels immediately following pulsed laser exposure. In this report, preliminary studies are described which demonstrate the potential application of IRT in the clinical management of PWS patients.

INTRODUCTION

Although the flashlamp-pumped pulsed dye laser has offered a superior approach in therapy due to its ability to destroy port-wine-stain (PWS) blood vessels selectively (1–3), only a small proportion of patients obtain 100% fading of their PWS, even after undergoing multiple laser treatments (4–7). One reason for poor results or treatment failure may be the lack of specificity in choosing the optimal pulse duration and light dosage to be delivered. Now that laser systems with user-specified pulse durations and light dosages are available commercially, how will the clinician select the optimal parameters for laser exposure?

Infra-red tomography (IRT) uses a fast infra-red focal plane array (IR-FPA) camera to detect temperature rises in a substrate induced by pulsed radiation. The temperature rise, due to the selective optical absorption of pulsed laser light, creates an increase in infra-red (blackbody) emission which is measured by a fast IR-FPA. For the purposes of IRT, chromophores in human skin can be modelled as a three-dimensional distribution of subsurface absorbing structures. In this model, when a pulsed laser source is used to irradiate the skin, an immediate increase in infra-red emission will occur due to heating caused by optical absorption in the chromophores. The absorbing chromophore's physical dimensions are best resolved in initial infra-red emission images when thermal diffusion is limited. Infra-red emission in later images is distributed more uniformly in space due to thermal diffusion.

An IRT record of human skin in response to pulsed laser exposure is composed of a time sequence of infra-red emission images that indicate localized heating of the subsurface chromophores. Analysis of the images contained within the IRT record at each PWS site by a tomographic reconstruction algorithm provides information on: (1) the depths and physical dimensions of discrete subsurface PWS blood vessels in human skin; and (2) the

0268–8921/96/030199+06 $12.00/0

initial space-dependent temperature increase in PWS blood vessels immediately following pulsed laser exposure (8). Such information can be used by the clinician to select the optimal laser pulse duration and light dosage on an individual patient basis throughout an extended treatment protocol. In this report, preliminary studies are described which demonstrate the potential application of IRT in the clinical management of PWS patients.

MATERIALS AND METHODS

The IRT integral equation, Equation 1(a), can be written as a multi-dimensional convolution integral that relates the measured time sequence of infra-red emission images, $\Delta M(x,y;t)$ (°C), where x,y;t are the tissue surface coordinates and time, respectively, to the initial space-dependent temperature increase, $\Delta T_{BV}(\xi,\eta,\zeta;t=0)$ (°C), of discrete subsurface PWS blood vessels at position (ξ,η,ζ), immediately following pulsed laser exposure (pulse ends at t=0):

$$\Delta M(x,y;t) = \iint_{x',y'} K_C(x-x',y-y')dx'dy' \iiint_{\xi,\eta,\zeta} K_T(x'-\xi,y'-\eta,\zeta;t)\Delta T_{BV}(\xi,\eta,\zeta;t=0)d\xi d\eta d\zeta \quad (1a)$$

Formally, this equation can be written as a product of two convolution operations, Equation 1(b), one (K_c) acting over the surface, and the other (K_T) inside the tissue:

$$\Delta M = K_C * K_T * \Delta T_{BV} \quad (1b)$$

where $K_c(x\text{-}x',y\text{-}y')$ (m^{-2}) and $K_T(x\text{-}\xi,y\text{-}\eta,\zeta;t)$ (m^{-3}) represent, respectively, the camera and thermal point spread (ie Green's) functions.

The camera point spread function (K_C) describes the inherent limitations of the IR-FPA camera which includes effects due to size of the collection aperture, lens aberrations, finite number and size of discrete detector elements.

Assuming a Dirac delta thermal source of unit strength embedded in a biological material at coordinates (ξ,η,ζ), solution of the bio-heat equation gives the thermal point spread function K_T:

$$K_T(x-\xi,y-\eta,\zeta;t) = K_r(x-\xi,y-\eta;t) \cdot K_z(\zeta;t) \quad (2)$$

where K_T is the product of two terms Equation 3(a,b), representing, respectively, heat diffusion along lateral [K_r (m^{-2})] and longitudinal [K_z (m^{-1})] axes (9).

$$K_r(x-\xi,y-\eta;t) = \frac{1}{\pi(2\sigma_s^2+4\chi t)} \exp[-((x-\xi)^2 + (y-\eta)^2)/(2\sigma_s^2+4\chi t)] \quad (3a)$$

$$K_z(t;\zeta) = \frac{\mu_{ir}\exp(-\zeta^2/4\chi t)}{2}\left\{\operatorname{erfcx}(u_+) + \operatorname{erfcx}(u_-) - \frac{2(h/\kappa)}{(h/\kappa)-\mu_{ir}}\cdot[\operatorname{erfcx}(u_+) - \operatorname{erfcx}(u_l)]\right\} \quad (3b)$$

where:

$$u_\pm = \mu_{ir}\sqrt{\chi t} \pm \frac{\zeta_o}{2\sqrt{\chi t}}, \quad u_l = \frac{h}{\kappa}\sqrt{\chi t} + \frac{\zeta_o}{2\sqrt{\chi t}} \quad (3c)$$

ζ_o, σ_s, χ, h and κ represent, respectively, depth of the thermal source, infra-red scattering length (mm), thermal diffusivity ($mm^2\ s^{-1}$), heat loss coefficient ($W\ m^{-2}\ K^{-1}$), and thermal conductivity of human skin ($W\ m^{-1}\ K^{-1}$). Furthermore, $\operatorname{erfcx}(u)=\exp(u^2)\operatorname{erfc}(u)$, where erfc(u) is the complementary error function [1-erf(u)].

The IRT integral Equation 1(a) represents a forward problem in which a time sequence of measured infra-red emission images [$\Delta M(x,y;t)$] may be computed from the initial space-dependent temperature increase, $\Delta T_{BV}(\xi,\eta,\zeta;t=0)$, and the known biophysical properties of human skin. Inasmuch as only $\Delta M(x,y;t)$ is available as input data, determination of $\Delta T_{BV}(\xi,\eta,\zeta;t=0)$ in the IRT integral Equation 1(a) constitutes an ill-posed mathematical inverse problem (Equation 4):

$$\Delta T_{BV} = (K_z)^{-1} \cdot (K_C * K_r)^{-1}\Delta M \quad (4)$$

Computationally efficient one-dimensional longitudinal inversion and two-dimensional lateral deconvolution algorithms have been developed to eliminate the effects of lateral heat diffusion and limited camera spatial resolution on $\Delta M(x,y;t)$. Such an approach permits reconstruction of an image of individual blood vessels immediately after the laser pulse is delivered. Furthermore, whereas the space-dependent temperature increase is always positive (ie $\Delta T_{BV} \geq 0$), a non-negative constrained conjugate gradient algorithm is used for improved solution estimates (10).

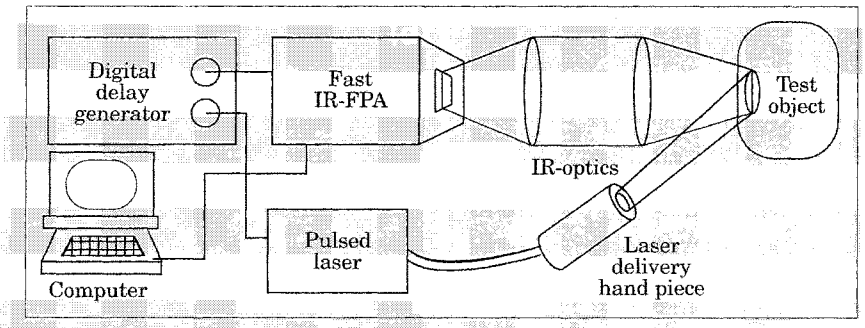

Fig. 1. Schematic diagram of infra-red tomography instrumentation. IR-FPA, infra-red focal plane array.

A number of preliminary experiments have been conducted on PWS patients that test the performance of the authors' non-negative constrained conjugate gradient longitudinal inversion and lateral deconvolution algorithms. A compound infra-red lens (f/5, 50 mm diameter) imaged the surface increase in infra-red emission intensity from the PWS skin on to a 128 × 128 InSb IR-FPA (Fig. 1). The camera system acquired 217 infra-red emission images per second and was triggered externally by a digital delay generator that was triggered optically by a fast silicon photo receiver. The infra-red signal collected by each detector element was digitized with a 3.5 MHz 12-bit (0-4,095) A/D converter and stored in the computer's random access memory. Immediately following exposure ($\lambda = 585$ nm; $\tau_p = 0.45$ ms; spot diameter 5 mm), the IR-FPA camera system acquired a time sequence of infra-red emission images $\Delta M(x,y;t)$.

Temperatures as recorded in infra-red emission frames $\Delta M(x,y;t)$ were calibrated for each IRT experiment. A resistor-heated aluminum surface coated with highly emissive ($\varepsilon > 0.967$) black paint was positioned in object space at the conjugate plane of the IR-FPA. A surface mount thermistor measured the temperature (sensitivity 0.01 °C) as the surface was heated slowly (1 °C min^{-1}). Calibration data matched closely the curve derived from Planck's law.

Twelve subjects were recruited for this ongoing evaluation from an on-site population of PWS patients at the Beckman Laser Institute and Medical Clinic, University of California, Irvine, USA. Permission to conduct the experimental protocol was obtained from the Human Subjects Review Committee Medical (Institutional Review Board). Port-wine-stain test sites were selected on inconspicuous sectors of the PWS (eg under the arm) that were representative of the entire lesion.

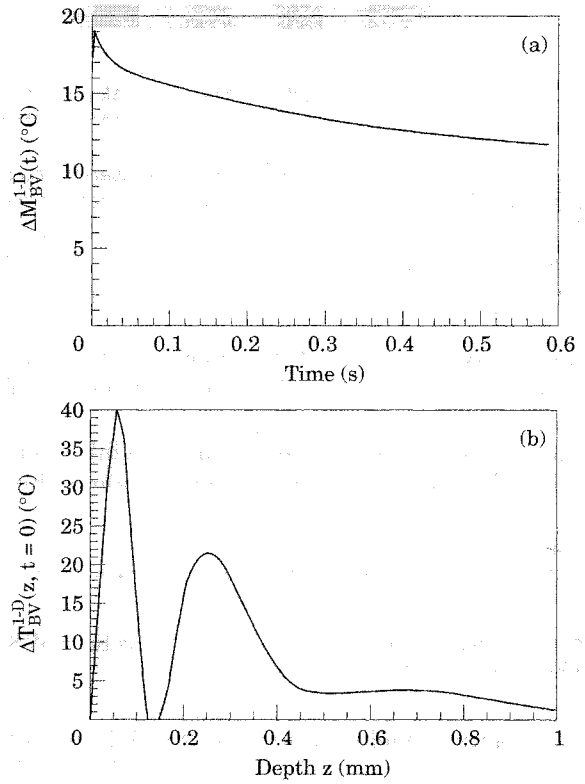

Fig. 2. (a) Measured infra-red emission, DM1-D/BV(t). (b) Depths of the epidermal melanin layer (50±25 μm) and port-wine-stain blood vessels (275±75 μm) determined by longitudinal inversion algorithm match the mean depths measured directly using histopathology.

RESULTS

Immediately following exposure to a 1.0 J laser pulse (5.0 J cm^{-2}), a timed sequence of 100 infra-red emission frames $\Delta M(x,y;t)$ was recorded over 460 ms with the IR-FPA camera system. From this sequence, the one-dimensional quantity $\Delta M1\text{-}D/BV(t)$ was determined [Fig. 2(a)] by averaging over an area ($\delta A = 1.5$ mm^2) positioned at the centre of laser exposure. Using the non-negative constrained conjugate gradient algorithm, the longitudinal inverse problem was solved [Fig. 2(b)] for the

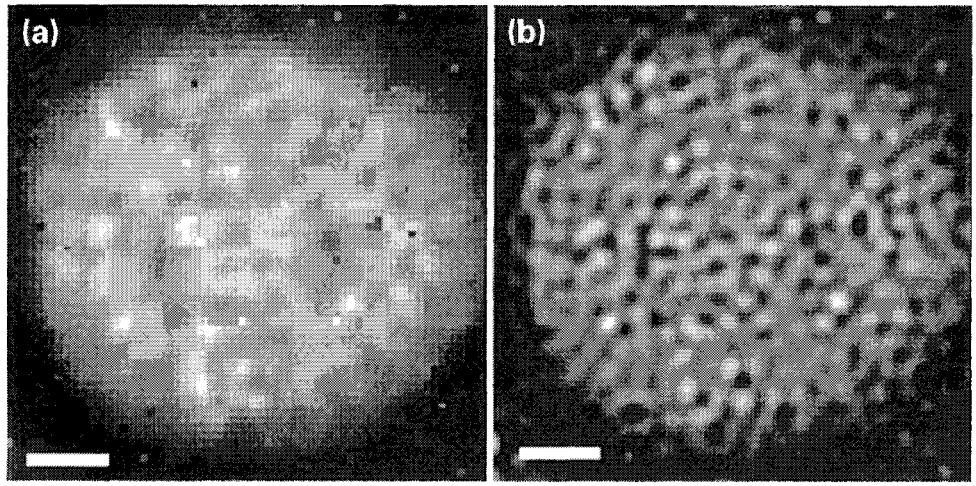

Fig. 3. (a) Measured infra-red emission image $\Delta M_{BV}(x,y;t_0=77\ ms)$. (b) Infra-red emission exclusively from the deeper discrete port-wine-stain blood vessels is computed by subtracting from $\Delta M_{BV}(x,y;t_0=77\ ms)$ the infra-red emission due to epidermal melanin heating. Solution of the lateral deconvolution problem (ΔT2-D/BV) allows determination of the lateral physical dimensions (150–200 μm) of discrete laser-heated subsurface PWS blood vessels. The mean temperature increase ($\Delta T_o=48\ °C$) of laser-heated discrete PWS blood vessels was computed from the fractional blood vessel area (f=0.42) in the deconvolved infra-red emission image and one-dimensional temperature increase [ΔT1-D/BV(z,t=0)] as determined from, respectively, the solutions of the lateral deconvolution and longitudinal inversion algorithms.

initial one-dimensional temperature increase, ΔT1-D/BV(z,t=0), in the epidermal melanin layer and deeper PWS blood vessels. Depths of the epidermal melanin layer ($50 \pm 25\ \mu m$) and deeper PWS blood vessels ($275 \pm 75\ \mu m$) determined by the longitudinal inversion algorithm [Fig. 2(b)] match the mean depths measured directly using histopathology (11).

For the same PWS site, $\Delta M_{BV}(x,y;t_0=77\ ms)$ was measured [Fig. 3(a)]. Infra-red emission exclusively from the deeper discrete PWS blood vessels is computed by subtracting from $\Delta M_{BV}(x,y;t_0=77\ ms)$ the infra-red emission due to epidermal melanin heating (8). Solution of the lateral deconvolution problem (ΔT2-D/BV) using the subtracted image as input data allows determination of the lateral physical dimensions (150–200 μm) of discrete laser-heated subsurface PWS blood vessels [Fig. 3(b)]. The mean temperature increase ($\Delta T_o=48\ °C$) of laser-heated discrete PWS blood vessels was computed from the fractional blood vessel area (f=0.42) in the deconvolved infra-red emission image and one-dimensional temperature increase [ΔT1-D/BV(z,t=0)] as determined from, respectively, the solutions of the lateral deconvolution and longitudinal inversion algorithms.

DISCUSSION

Histopathological studies of PWS show a plexus of layers of dilated blood vessels located below the skin surface in the upper dermis. Port-wine-stain blood vessel diameters vary on an individual patient basis, and even from site to site on the same patient over a range of 10–150 μm (12). The thermal relaxation time (τ_r) is defined as the time required for the core temperature, produced by the absorbed light energy within the target blood vessel, to cool to one-half of its original value immediately after the laser pulse and may be expressed:

$$\tau_r = \frac{d_{BV}^2}{16\chi} \qquad (5)$$

where d_{BV} is the diameter of the targeted blood vessel and χ is the thermal diffusivity of skin ($0.11\ mm^2\ s^{-1}$). For vessels with diameters of 10, 70 and 150 μm, τ_r has calculated values of 0.06, 2.8 and 12.8 ms, respectively. The pulse duration of laser exposure (t_p) governs the spatial confinement of heat and should, ideally, match the thermal relaxation time (τ_r) for the targeted blood vessels (13). If longer pulse durations are employed ($t_p \gg \tau_r$), heat diffuses outside the vessel during laser exposure. The target specificity is reduced resulting in non-specific thermal damage to adjacent structures. Alternatively, if too short a laser pulse is used ($t_p \ll \tau_r$), high-peak intravascular temperature rises can produce explosive vaporization of tissue water, or photo-acoustic transients which can result in vessel rupture. In such cases, repair mechanisms may revascularize the PWS. In conclusion, selection of the

correct pulse duration of laser exposure is crucial to successful blood vessel destruction. Only when $t_p \approx \tau_r$ can the critical core intravascular temperature, necessary to destroy large PWS blood vessels irreversibly, be achieved and sustained for sufficient time (14, 15).

It is important to be aware that like pulse duration, light dosage (J cm^{-2}) is also dependent on blood vessel diameter. For larger vessels, as energy deposition is limited by the optical penetration depth in whole blood ($\mu^{-1}_a = 30\,\mu m$ at 585 nm), higher light dosages must be administered to reach, and sustain for sufficient time, the necessary critical core intravascular temperature (16, 17). Therefore, for the clinician to select the optimal light dosage as a function of pulse duration correctly, knowledge of the initial space-dependent temperature increase in subsurface PWS blood vessels [$\Delta T_{BV}(\xi,\eta,\zeta;t=0)$] immediately following pulsed laser exposure is required.

For laser pulses in the millisecond domain, irreversible damage to PWS blood vessels is assumed to occur at core temperatures higher than 80 °C (16). Once $\Delta T_{BV}(\xi,\eta,\zeta;t=0)$ has been determined from the IRT record in response to a diagnostic sub-therapeutic laser pulse of duration t_0 and light dosage D_0, the therapeutic laser light dosage (D_{PWS}) necessary to destroy the PWS blood vessels can be computed appropriately from Equation 6 knowing the critical temperature increase, $\Delta T_C = 50$ °C (assuming an ambient skin temperature of 30 °C).

$$D_{PWS} \cong D_0 \frac{\Delta T_C}{\Delta T_{BV}} \frac{t_p}{t_o} \frac{(1-e^{-t_0/\tau_r})}{(1-e^{-t_p/\tau_r})} \qquad (6)$$

The rationale for using IRT in the clinical management of patients with PWS is that the technique offers a means of documenting the vascular characteristics of PWS on a site-to-site basis for each patient. Prior to the institution of laser therapy, in response to a sub-therapeutic diagnostic laser pulse, analysis of the measured time sequence of emission images [$\Delta M(x,y;t)$] contained within the IRT record at each PWS site by the tomographic reconstruction algorithm provides information on: (1) the depths and physical dimensions of the most superficial absorbing PWS blood vessels inside the beam spot of uniform light intensity; and (2) the initial space-dependent temperature increase [$\Delta T_{BV}(\xi,\eta,\zeta;t=0)$] within the blood vessels immediately following pulsed laser exposure. Such information can be used by the clinician to help select the optimal parameters (pulse duration and light dosage) for the first laser treatment. Once the mean diameter of PWS blood vessels (d_{BV}) inside the beam spot is determined from the deconvolved image, t_p can be calculated (14, 18). With $\Delta T_{BV}(\xi,\eta,\zeta;t=0)$ determined, the therapeutic laser light dosage (D_{PWS}) to destroy the PWS blood vessels can be computed from Equation 6. At the next patient visit, a second IRT record is made. As the majority of the most superficial PWS blood vessels were obliterated by the first laser treatment, the diagnostic laser pulse now images a deeper absorbing layer of PWS blood vessels. The optimal parameters (pulse duration and light dosage) for the second laser exposure are selected based on analysis of the IRT record, and a second treatment is performed. Proceeding in this manner, the IRT record probes deeper and deeper absorbing layers of the PWS after the most superficial layers are removed by each successive treatment at the same site. In conclusion, information provided by IRT can be used by the clinician to select the optimal laser pulse duration and light dosage on an individual patient basis throughout an extended treatment protocol.

ACKNOWLEDGEMENTS

This work was supported by research grants awarded from the Biomedical Research Technology Program (R03-RR06988) and Institute of Arthritis and Musculoskeletal and Skin Diseases (1R29-AR41638-01A1 and 1R01-AR42437-01A1) at the National Institutes of Health, Whitaker Foundation and Dermatology Foundation. Institutional support from the Office of Naval Research, Department of Energy, National Institutes of Health, and the Beckman Laser Institute and Medical Clinic (BLIMC) Endowment is also acknowledged gratefully. Financial support for the sabbatical leave of Martin van Gemert at the BLIMC is from the Dutch Technology Foundation (STW Grant AGN33.2954) and the Academic Medical Center, University of Amsterdam.

REFERENCES

1 Ashinoff R, Geronemus RG. Flashlamp-pumped pulsed dye laser for port wine stains in infancy: earlier versus later treatment. *J Am Acad Dermatol* 1991, **24**:467–72
2 Nelson JS, Applebaum J. Clinical management of port-wine stain in infants and young children using the flashlamp-pulsed dye laser. *Clin Pediatrics* 1990, **29**:503–8
3 Tan OT, Morrison P, Kurban AK. 585 nm for the treatment of port-wine stains. *Plast Reconstr Surg* 1990, **86**:1112–7

4 Garden JM, Polla LL, Tan OT. The treatment of port wine stains by the pulsed dye laser. *Arch Dermatol* 1988, **124**:889–96
5 Reyes BA, Geronemus RG. Treatment of port-wine stains during childhood with the flashlamp-pumped dye laser. *J Am Acad Dermatol* 1990, **23**:1142–8
6 Ashinoff R, Geronemus RG. Capillary hemangiomas and treatment with the flashlamp-pulsed dye laser. *Arch Dermatol* 1991, **127**:202–5
7 Geronemus RG. Pulsed dye laser treatment of vascular lesions in children. *J Dermatol Surg Oncol* 1993, **19**:303–10
8 Nelson JS, Milner TE, Tanenbaum BS, Goodman DM. Space dependent temperature increase in human skin subsurface chromophores immediately following pulsed laser exposure. *SPIE* 1996, **2623**:20–31
9 Milner TE, Goodman DM, Tanenbaum BS, Anvari B, Svaasand LO, Nelson JS. Imaging laser heated subsurface chromophores in biological materials: determination of lateral physical dimensions. *Phys Med Biol* 1996, **41**:31–44
10 Goodman DM, Johansson E, Lawrence TW. On applying the conjugate-gradient algorithm image processing problems. In: Rao CR (ed) *Multivariate Analysis: Future Directions*. Amsterdam: North-Holland Press, 1992
11 Milner TE, Smithies D, Goodman DM, Lau A, Belson JS. Depth determination of chromophores in human skin by pulsed photothermal radiometry. *Appl Optics* 1996, **35**:3314–20
12 Barsky SH, Rosen S, Geer DE, Noe JM. The nature and evolution of port wine stains: a computer assisted study. *J Invest Dermatol* 1980, **74**:154–7
13 Anderson RR, Parrish JA. Selective photothermolysis: precise microsurgery by selective absorption of pulsed radiation. *Science* 1983, **220**:524–7
14 de Boer JF, Lucassen GW, Verkruysse W, van Gemert MJC. Thermolysis of port-wine-stain blood vessels: diameter of a damaged blood vessel depends on the laser pulse length. *Lasers Med Sci* 1996, **11**:177–80
15 Svaasand LO, Fiskerstrand EJ, Kopfstad G et al. Therapeutic response during pulsed laser treatment of port-wine stains; dependence on vessel diameter and depth in dermis. *Lasers Med Sci* 1995, **10**:235–43
16 van Gemert MJC, Welch AJ, Miller ID, Tan OT. Can physical modeling lead to an optimal laser treatment strategy for port-wine stains? In: Wolbarsht M (ed) *Laser Applications in Medicine and Biology*. New York: Plenum Press, 1991:199–275
17 Kimel S, Svaasand LO, Hammer-Wilson M et al. Differential vascular response to laser photothermolysis. *J Invest Dermatol* 1994, **103**:693–700
18 van Gemert MJC, Nelson JS, Milner TE et al. Noninvasive determination of port wine stain anatomy and physiology for optimal laser treatment strategies. *Physics Med Biol* 1996, in press

Key words: Port-wine stain; Infra-red tomography; Laser treatment; Blood vessel; Photothermolysis